JBC Papers in Press. Published on August 15, 2016 as Manuscript M116.748186
The latest version is at http://www.jbc.org/cgi/doi/10.1074/jbc.M116.748186

MICAL3 flavoprotein monooxygenase forms a complex with centralspindlin and regulates cytokinesis.

Qingyang Liu [1], Fan Liu[2], Ka Lou Yu [1,3], Roderick Tas [1], Ilya Grigoriev [1], Sanne Remmelzwaal [1], Andrea Serra-Marques [1,4], Lukas C. Kapitein[1], Albert J. R. Heck [2] and Anna Akhmanova [1]

[1] Cell Biology, Faculty of Science, Utrecht University, Padualaan 8, 3584 CH Utrecht, the Netherlands

[2] Biomolecular Mass Spectrometry and Proteomics, Bijvoet Center for Biomolecular Research and Utrecht Institute for Pharmaceutical Sciences, Utrecht University, 3584 CH Utrecht, the Netherlands

[3] Present address: Institute of Medical Biology, Agency for Science, Technology, and Research, Singapore, 8a Biomedical Grove, 06-06, Immunos, Singapore 138648

[4] Present address: Department of Cell & Tissue Biology, University of California San Francisco, San Francisco, CA, United States of America

Running title: *MICAL3 in cytokinesis*

To whom the correspondence should be addressed: Prof. Dr.A. Akhmanova, Cell Biology, Faculty of Science, Utrecht University, Padualaan 8, 3584 CH Utrecht, the Netherlands, Telephone: +31-30-2532328; FAX: +31-30-2532837; E-mail:a.akhmanova@uu.nl

Keywords: Cytokinesis, actin; microtubule, protein cross-linking, mass spectrometry (MS), midbody, centralspindlin, vesicle transport, flavoprotein monooxygenase

ABSTRACT

During cytokinesis, the antiparallel array of microtubules forming the central spindle organizes the midbody, a structure that anchors the ingressed cleavage furrow and guides the assembly of abscission machinery. Here, we identified a role for the flavoprotein monooxygenase MICAL3, an actin disassembly factor, in organizing midbody-associated protein complexes. By combining cell biological assays with cross-linking mass spectrometry, we show that MICAL3 is recruited to the central spindle and the midbody through a direct interaction with the centralspindlin component MKLP1. Knockout of MICAL3 leads to an increased frequency of cytokinetic failure and a delayed abscission. In a mechanism independent of its enzymatic activity, MICAL3 targets the adaptor protein ELKS and Rab8A-positive vesicles to the midbody, and the depletion of ELKS and Rab8A also leads to cytokinesis defects. We propose that MICAL3 acts as a midbody-associated scaffold for vesicle targeting, which promotes maturation of the intercellular bridge and abscission.

Cytokinesis is the last step of cell division, during which the cytoplasm is partitioned between the two daughter cells. In animal cells, the major steps of cytokinesis are the formation of the actomyosin ring and its contraction, resulting in the ingression of the cleavage furrow, formation of an intercellular bridge and its subsequent scission (1-2). At the onset of cytokinesis, microtubules at the spindle midzone arrange into an overlapping antiparallel array, the central spindle, which first forms a signaling platform important for the positioning of the cleavage plane and later organizes the midbody, an electron-dense structure that anchors the ingressed furrow and guides the assembly of abscission machinery (1-3).

One of the major players in the assembly and function of the central spindle is the centralspindlin complex, composed of the kinesin-

6 family protein Mitotic Kinesin-Like Protein 1 (MKLP1, also known as KIF23 in mammals) and the Rho GTPase activating protein CYK-4 (also known as or MgcRacGAP) (4). Centralspindlin participates in bundling antiparallel microtubules of the central spindle, activation of the Rho GTPase, which controls formation of the actomyosin ring, and the formation of the midbody (4).

Membrane trafficking, including both endosomes and secretory carriers, also plays an important role in cytokinesis (5-7). The small GTPase Rab8, known to label both endosomal and secretory vesicles (8-11), prominently accumulates at the midbody (12-14), and its transport to the intercellular bridge is directed by cytoplasmic dynein and the doublecourtin domain-containing protein-5 (12). The docking and fusion of Rab8-positive secretory vesicles with the plasma membrane depends on the cortical complex which contains a coiled coil adaptor ELKS/ERC1 (15) and the flavoprotein monooxygenase enzyme MICAL3 (8). The members of the MICAL family, which in mammals includes MICAL1, MICAL2 and MICAL3, are best known for their ability to promote actin disassembly by oxidizing specific methionine residues (16-18). In addition, MICAL1 and MICAL3 can bind to multiple members of the Rab GTPase family, including Rab8 (8,19), but the exact function of these interactions is poorly understood.

Here, we searched for new binding partners of MICAL3 and identified the two components of the centralspindlin complex among the highest hits. Since centralspindlin is a major player during cytokinesis, we hypothesized that MICAL3 also participates in this process. We tested this possibility using a combination of biochemical and cell biological experiments and found that MICAL3 is indeed required for cytokinesis. We showed that MKLP1 recruits MICAL3 to the central spindle, while MICAL3 participates in targeting to the midbody its binding partners ELKS and Rab8A, and the loss of both ELKS and Rab8A also caused cytokinesis defects. Interestingly, the cytokinetic function of MICAL3 appeared not to require its enzymatic activity. Our data suggest that MICAL3 plays a role in organizing membrane trafficking at the intercellular bridge and that it acts in this process not as an actin disassembly factor but as a protein-binding hub.

RESULTS

MICAL3 interacts with MKLP1

To get insight into the function of MICAL3, we performed a mass spectrometry-based screen for its binding partners. We co-expressed in HEK293T cells the biotin ligase BirA together with MICAL3 carrying a bioGFP tag, which consists of GFP with an N-terminally attached artificial peptide that can be efficiently biotinylated by BirA (20), and performed streptavidin pull down assays from the lysates of these cells. BioGFP alone was used as a negative control. MICAL3 was the highest specific hit in this experiment, and the already known partners of MICAL3, ELKS (ERC1) and Rab8A, were also identified with high confidence (Fig. 1A). We also identified α- and β-spectrins (SPTAN and SPTBN1; Fig.1A), which are large cortical proteins involved in the control of mechanical stability of cellular membranes and assembly of cortical cytoskeleton and specialized membrane domains (21-23). Since MICAL3 can regulate actin disassembly, its binding to spectrins might play a role in controlling the organization of the cortical actin networks.

Among the other major hits in this screen were the two components of the centralspindlin complex, MKLP1 (KIF23) and CYK-4 (RACGAP) (Fig. 1A). The validity of the interaction with centralspindlin is supported by the fact that MICAL3 was previously reported as one of the potential partners of MKLP1 in HeLa cells in a high-throughput screen (24).

To investigate the interaction between MICAL3 and MKLP1 in more detail, we performed cross-linking mass spectrometry experiments. BioGFP-MICAL3 was co-expressed in HEK293 cells together with GFP-MKLP1 and BirA, biotinylated proteins were isolated by streptavidin pull down, cross-linked on beads using disuccinimidyl sulfoxide (DSSO) and the cross-linked peptides were analyzed by mass spectrometry as described previously (25). We identified multiple cross-links within both MICAL3 and MKLP1. The cross-links within folded domains of known structure (MICAL1 monooxygenase, MKLP1 C-terminus) were in good agreement with the DSSO distance constraint

of 28.4 Å (23.4 Å for the maximal distance constraint of the DSSO cross-linker plus 5 Å tolerance for protein flexibility in solution), validating our cross-linking mass spectrometry approach (Fig. 1B,C, Table S1). We also found many cross-links between different domains of MICAL3, compatible with the previously proposed autoinhibitory folding of MICAL proteins (Fig. 1B, Table S1)(8,26).

Specific cross-links were also observed between the second and third coiled coil region of MICAL3 and the coiled coil and the adjacent C-terminal domain of MKLP1 (Fig. 2A, Fig. 1C, Table S1). Pull down assays confirmed the cross-linking results and showed that the minimal MKLP1-binding domain of MICAL3 encompasses its C-terminal coiled coil region (MICAL3-CC4), while a stronger interaction was observed with a larger C-terminal fragment, which includes all the cross-linked sites (MICAL3-CC3, Fig. 2B-E). Since the C-termini of MICAL1 and MICAL3 are quite similar, we have also tested whether MICAL1 can interact with MKLP1, but found that this was not the case (Fig. 2D).

The minimal MICAL3-binding domain of MKLP1 was present in the strongly charged and likely unstructured region located at the C-terminal side of the coiled coil of MKLP1 (Fig. 2A, Fig.3A-C). By deletion mapping, we identified a region of 13 residues which was essential for the interaction (mutant D7), while the deletion of the adjacent 15 amino acid region (mutant D8) did not perturb the binding (Fig. 3A, D, Fig. 1C, Table S1). Taken together, our results show that MKLP1 and MICAL3 primarily interact through the unstructured polypeptide region in MKLP1 and the C-terminal coiled coil of MICAL3, with additional contacts provided by the second coiled coil domain of MICAL3 and the coiled coil domain of MKLP1.

MKLP1 recruits MICAL3 to the central spindle and the midbody

We next examined the localization of endogenous MICAL3 in mitotic cells and found that while no conspicuous localization of MICAL3 could be detected at the early cell division stages, MICAL3 was clearly enriched at the spindle midzone starting from anaphase and strongly accumulated at the central spindle and the midbody during cytokinesis (Fig. 4A). Fluorescently tagged MICAL3 colocalized with the endogenous MKLP1 at the central spindle and the midbody (Fig. 4B). This localization did not depend on the enzymatic activity of MICAL3 as it was observed with the enzymatically dead MICAL3 mutant (Fig. 4C). Importantly, in MKLP1-depleted cells, MICAL3 failed to localize to the spindle midzone, indicating that MKLP1 targets MICAL3 to this location (Fig. 4D-G).

We next set out to test whether MICAL3 affects the localization of MKLP1. Since we did not manage to achieve an efficient siRNA-mediated knockdown of MICAL3, we used CRISPR/Cas9 mediated knockout technology. Cells transfected with a vector co-expressing a puromycin resistance gene, a single guide RNA sequence specific for MICAL3 and Cas9 (27) were subjected to puromycin selection and analyzed at 6-7 days after transfection to avoid the selection of cells, in which the potential cell division defects would be compensated by secondary mutations. This procedure led to highly efficient knockout of MICAL3 protein expression (Fig. 4H). We found that the loss of MICAL3 had no effect on MKLP1 binding to the central spindle or the midbody (Fig. 4I). We conclude that MICAL3 is recruited to sites of centralspindlin accumulation but has no effect on its distribution.

MICAL3 is required for cytokinesis

To determine whether the loss of MICAL3 affects cell division, we performed phase contrast-based live imaging experiments and found that compared to the cells transfected with the vector alone, MICAL3 knockout cells displayed a slight delay between the mitotic onset and the initiation of furrow ingression, and a very significant (more than twofold) increase in the time between the completion of furrow ingression and abscission (Fig. 5A-C, Movie S1, S2). We observed no abnormalities during the formation or ingression of the cleavage furrow and detected no visible defects in the organization of the actin cytoskeleton during different mitotic stages, including cytokinesis (Fig. 6A,B). The data indicate that the actin-depolymerizing activity of MICAL3 is unlikely to contribute to the dynamics of the actomyosin ring. We did, however, observe a significant increase in the percentage of cells that fused back after furrow ingression and the corresponding increase in the percentage of

binucleated cells (from ~2% to ~10%) (Fig. 5A,D,E, Movie S3). To test whether this effect of MICAL3 was specific, we performed rescue experiments with GFP-tagged MICAL3 expression constructs (Fig. 5F). While no rescue was observed with GFP alone, we could completely rescue the binucleated phenotype by either the full length MICAL3 or its enzymatically dead mutant, but not with the MICAL3 deletion mutant lacking the MKLP1-binding C-terminus (Fig. 5F). Thus, these data indicate that MICAL3 contributes to the stabilization and/or maturation of the intercellular bridge in a way that does not require its monooxygenase activity.

For comparison, we examined the phenotype of MKLP1 depletion and found that, as expected, its effect on cytokinesis was much more profound than that of MICAL3 knockout, with ~70 % of binucleated cells (Fig. 5G). We observed a very significant though not complete rescue of this phenotype by expressing GFP-MKLP1 (Fig. 5G). The MKLP1 deletion mutant D7, which was unable to bind to MICAL3 and promote MICAL3 localization to the midbody (Fig. 3D, Fig.5H), performed significantly less well in the rescue experiments than the wild type MKLP1 and the MKLP1-D8 mutant, which could restore MICAL3 accumulation at the midbody in MKLP1-depleted cells (Fig. 5G,H). While we cannot exclude that the D7 mutant perturbs MKLP1 function in ways unrelated to MICAL3 binding, our results are fully compatible with a role of MKLP1-dependent recruitment of MICAL3 as a factor contributing to the successful completion of cytokinesis.

MICAL3 promotes the recruitment of ELKS and Rab8 to the intercellular bridge

Since our data indicated that the contribution of MICAL3 to cytokinesis does not require its actin-destabilizing monooxygenase activity, we turned our attention to its binding partners. We first examined the distribution of ELKS, which was shown previously to bind to MICAL3 and participate in secretory vesicle docking (8). We found that ELKS prominently localized to the midbody in 90% of the cells, and that this localization was completely lost in MICAL3 knockout cells (Fig. 7A, B). Since MICAL3 is targeted to the midbody by MKLP1, these results suggest that MICAL3 might be able to connect ELKS to MKLP1. In support of this, mass spectrometry-based analysis of BioGFP-ELKS pull downs from HEK293 cells identified MKLP1 (KIF23) as a potential interacting partner (Fig. 7C). We next tested whether the interaction between MKLP1 and ELKS is mediated by MICAL3 and found that co-expression of MICAL3 indeed enhanced the ability of MKLP1 to co-precipitate ELKS (Fig. 7D). We conclude that MICAL3 can form a triple complex with MKLP1 and ELKS and through the interaction with the former, target the latter to the midbody.

We have also examined the distribution of Rab8A-labeled membranes. Rab8A was present at ~75% of the midbodies (Fig. 8A,B). The intercellular bridges lacking Rab8A-positive structures appeared to represent very late stages of cytokinesis, in line with previous publications showing that Rab8A-positive vesicles are removed from the intercellular bridge prior to abscission (13-14). The percentage of cells that exhibited at least some Rab8A signal at the intercellular bridge was significantly reduced in MICAL3 knockout cells (Fig. 8A,B), and the intensity of Rab8A staining in the midbody region was also reduced (Fig. 8C). In contrast, the localization of transferrin receptor-positive or Rab11-positive endosomes to the midbody was not perturbed by MICAL3 knockout (Fig. 8D,E). We conclude that MICAL3 specifically contributes to the recruitment of Rab8A to the midbody.

Mass spectrometry-based analysis of ELKS binding partners in HEK293 cells identified Citron kinase (CRIK) and its binding partner kinesin-3 KIF14 (Fig. 7C), while these proteins were not present in the MICAL3 pull down (Fig. 1A, Fig. 7C). We have examined whether the localization of CRIK or KIF14 was perturbed in MICAL3 knockout cells and found this not to be the case (Fig. 8F). While these data do not rule out that ELKS, localized to the midbody through its interaction with MICAL3, somehow affects the function of CRIK-containing protein complexes, they indicate that MICAL3 does not participate in the targeting of this signaling protein complex to the intercellular bridge, in line with the data showing that CRIK directly interacts with MKLP1 (28).

ELKS and Rab8 are required for cytokinesis

If the cytokinetic defect of MICAL3 knockout cells occurs due to the inability to properly localize ELKS and Rab8A-postive membranes, then the depletion of these proteins can be expected to perturb cytokinesis as well. We examined this possibility by depleting ELKS and knocking down ELKS and Rab8A (Fig. 8G,H); the two proteins were depleted by 75% and 95%, respectively. The intensity of Rab8A staining in the midbody region in ELKS-depleted cells was reduced to values close to background (Fig. 8A, I). The depletion of either ELKS or Rab8A led to a significant increase of binucleated cells (~10%, similar to MICAL3 knockout) (Fig. 8J,K). We conclude that the complex of MICAL3 and ELKS targets Rab8A to the intercellular bridge, and that all three proteins are required to the proper maturation of the bridge, which prevents the bridge recession and promotes timely abscission.

DISCUSSION

In this study we identified MICAL3 as a new molecular player in cytokinesis and a binding partner of MKLP1. Previous work has shown that centralspindlin represents a major binding hub for different factors involved in cytokinesis (4), and our current work added MICAL3 to the list of MKLP1 interactors. Cross-linking experiments combined with mass spectrometry allowed us to show that the MICAL3-MKLP1 association is direct and to characterize the contact sites between the two proteins, illustrating the power of this approach. The MICAL3-binding region of MKLP1 is distinct from the MKLP1 sites known to bind to CYK-4, ARF6 or 14-3-3, but there might be some overlap with the binding sites for CRIK and CEP55 (Fig. 3A) (28-32). The MKLP1 binding site of MICAL3 overlaps with that of Rab8A but is different from the region involved in the interaction with ELKS (8) (Fig. 2B), and in agreement with these data, we showed that MICAL3 can connect ELKS to MKLP1.

Our data indicate that MICAL3 is involved in stabilization and maturation of the intercellular bridge, because its loss led to increased frequency of cytokinetic failure and extended duration of abscission. Surprisingly, in spite of the well-established role of MICAL enzymes in actin disassembly, we found no evidence that MICAL3 regulates actin cytoskeleton during cytokinesis. Instead, MICAL3 recruits ELKS and Rab8A to the midbody (Fig. 9), and the depletion of these two proteins caused an increase of binucleated cells, indicative of cytokinetic defect. The function of MICAL3 in cytokinesis thus appears to be mechanistically similar to that of MICAL3-related protein MICAL-L1, which lacks an enzymatic domain, localizes to the midbody and plays a role in organizing recycling endosomes at the intercellular bridge (33).

The next challenge is to identify the exact molecular role of Rab8A vesicles in cytokinesis. Since these vesicles are cleared from the intercellular bridge before the actual abscission (13-14), we favor the idea that they transport molecules required for the maturation of the intercellular bridge and the midbody, such as some signaling factors. This function would be similar to that of Rab35, which contributes to actin depolymerization by delivering to the intercellular bridge the phosphoinositide phosphatase OCRL (34-35). The role of Rab8A vesicles in protein delivery to the midbody would be consistent with the observation that the enzymatic activity of MICAL3 is not essential for the cytokinetic function in spite of the fact that it promotes vesicle fusion with the plasma membrane.

The loss of MICAL3, ELKS and Rab8A caused a similar, relatively mild cytokinetic defect, with ~10% binucleated cells, indicating that the absence of these proteins can be compensated by other factors, at least in HeLa cells, though the situation might be different in other systems. It is possible that different vesicular populations at the midbody have partially overlapping functions. Although Rab8A can be recruited to Rab11-positive recycling endosomes (11), the MICAL3-dependent population of Rab8A vesicles at the midbody is distinct from Rab11-labeled endosomes, which were not affected by MICAL3 knockout. The Rab8A vesicles studied here might overlap with the post-Golgi carriers, which were previously described to participate in cytokinesis (36-37). Golgi-dependent secretory trafficking was shown to be necessary for cytokinesis during development in invertebrates (5,7), and a similar function might be also important in mammals, constituting a potentially interesting avenue for future studies.

Experimental Procedures

DNA constructs and siRNAs

We used the following previously described constructs: BioGFP-MICAL3-WT, mCherry-MICAL3-WT, BioGFP-MICAL3-3G3W and mCherry-MICAL3-3G3W (8). Deletion mutants of MICAL3 were cloned by PCR-based strategy. GFP-MKLP1 constructs were based on plasmids that were a gift from Dr. Stephen Doxsey (University of Massachussetts, USA) and M. Mishima (Warwick Medical School, UK). BioGFP-MICAL1-FL was a gift from Dr. R.J. Pasterkamp (UMC Utrecht, The Netherlands). GFP-Rab11 was purchased from Addgene (Plasmid #12674).

The target sequences of control and ELKS siRNAs were described previously (38). MKLP1 siRNA was described in (39). MICAL1 siRNA was synthesized by Ambion (ID: s230028). Rab8A siRNA corresponded to the target sequence GGAAAGCACAAATGAAGGA. Cells were transfected with 10 nM siRNAs using HiPerFect (Qiagen) and analysed 3 days after transfection.

Cell culture and CRISPR/Cas9-mediated knockouts

HEK293T and HeLa were cultured as described previously (8). We used FuGENE 6 (Promega) for plasmid transfection, and HiPerFect (Qiagen) for siRNA transfection of HeLa cells; polyethylenimine (PEI, Polysciences) was used to transfect HEK293T cells for streptavidin pull-down assays, which were performed as described previously (8).

The target sequence for CRISPR targeting of human MICAL3 gene was CCCCAGTAAGGATAAGTCGA (Exon 3). Two complementary oligonucleotides with BpiI restriction sites for guide RNAs (gRNAs) were synthesized, and cloned into pX459 CRISPR/Cas9-Puro vector (27) (Addgene, Cambridge, MA). HeLa cells were transfected with Px459 vector or pX459-MICAL3gRNA and treated with 2 μg/ml of puromycin for two days and analyzed within a 4-day period post puromycin treatment.

Antibodies and immunofluorescence cell staining

We used a homemade rabbit polyclonal antibodies against MICAL3, MKLP1 (Santa Cruz Biotechnology), GFP (Abcam, ab290), ELKS (Proteintech, 22211-1-AP), KIF14 (Bethyl Laboratories) and Rab8A (a gift of J. Peränen, University of Helsinki, Finland) (40). We used mouse monoclonal antibodies against mCherry (Clontech, 632543), β-tubulin (Sigma-Aldrich, T5201), $p150^{Glued}$ (BD Biosciences, 610474), actin (Chemicon), CRIK (BD Biosciences), Transferrin receptor (Bochringer) and rat monoclonal antibodies against α-tubulin YL1/2 (Pierce, MA1-80017). The following secondary antibodies were used: IRDye 800CW/ 680LT goat anti-rabbit, and anti-mouse (Li-Cor Biosciences); Alexa-488 and Alexa-594 conjugated goat antibodies against rabbit, rat and mouse IgG (Molecular Probes). The Alexa 594-conjugated phalloidin were purchased from Invitrogen.

To label proteins, cells were fixed with –20 °C methanol for 10 min or 3.7% paraformaldehyde in PBS for 10 min at room temperature. Cells were permeabilized with 0.1% Triton X-100 in phosphate-buffered saline (PBS) for 10 min; subsequent washing and labelling steps were carried out in PBS supplemented with 2% bovine serum albumin and 0.05% Tween-20. At the end, slides were rinsed in 70% and 100% ethanol or air-dried and mounted in Vectashield mounting medium (Vector laboratories).

Mass spectrometry

Sample preparation. Samples were prepared from pull-down assays of biotinylated proteins from extracts of transfected HEK293T cells using streptavidin beads, and were analysed by subsequent mass spectrometry experiments as described previously (8). For cross-linking experiment, the immunoprecipitated proteins were on-beads cross-linked using 1mM DSSO cross-linker (41). The cross-linking reaction was carried out for 1 hr at room temperature and quenched with 20 mM Tris-HCl (pH 7.8) for 30 min at room temperature. Subsequently, the on-beads cross-linked proteins were denatured with 2 mM urea, reduced with 4 mM dithiothreitol at 56 °C for 30 min and alkylated with 8 mM iodoacetamide at room temperature for 30 min in the dark. Proteins were digested using trypsin at an enzyme-to-protein ratio of 1:20 (w/w) at 37 °C for 2 hr. The supernatant was removed from the beads and further digested at 37 °C overnight. Protein digests were desalted using Sep-Pak C18 cartridges (Waters), dried and stored at −20 °C for further

use. The desalted digests were SCX fractionated as previously described (25), and only the late SCX fractions (predominantly containing higher charged species) were subjected to LC/MS analysis.

LC/MS/MS analysis. Peptides and cross-linked peptides were analyzed using an ultra HPLC Proxeon EASY-nLC 1000 system (Thermo Fisher Scientific) coupled on-line to an ETD enabled LTQ Orbitrap Elite mass spectrometer (Thermo Fisher Scientific). For cross-link analysis, reversed-phase separation and MS data acquisition were performed as previously described and data analysis was accomplished using XlinkX software (25). Results were filtered by 1% false discovery rate and all reported cross-links were manually validated. For peptide identification, rapid CID was used for data acquisition. Peptide identification was performed using Proteome Discoverer 1.4 (Thermo Fisher Scientific). Results were filtered by 1% false discovery rate.

Image Acquisition

Images of fixed cells were collected with a Nikon Eclipse 80i upright fluorescence microscope and a CoolSNAP HQ2 CCD camera (Photometrics), using a Nikon Plan Apo VC 60x/N.A.1.40 oil objective or Nikon Plan Apo VC 100x/ N.A.1.40 x oil objective .

Live-cell phase contrast imaging was performed on inverted research microscope Nikon Eclipse Ti-E (Nikon) with the perfect focus system (Nikon), equipped Nikon Plan Apochromat 20x/0.75 Phase Contrast objective (Nikon), a CoolSNAP HQ2 CCD camera (Photometrics) and controlled with Micro-Manager Open Source Microscopy Software (https://micro-manager.org/). To keep the cells at 37 °C, a stage top incubator model INUBG2E-ZILCS (Tokai Hit) was used. Images were projected onto the CCD chip at a magnification of 0.3215 µm/pixel. Round 25 mm coverslips were mounted in Attofluor Cell Chamber (Thermofisher) and maintained at 37 °C and 5% CO2. Cells were imaged every 2 min for 6-12 hr.

Confocal 300 nm Z-stack images were acquired on a Leica SP8 DMI STED microscope equipped with a 100x HC Pl Apo objective (Leica, NA 1.4. oil) and the Leica HyD detector controlled by the Leica Application Software X. Excitation of Alexa488, Alexa568 and Alexa647 was performed with a SuperK EXTREME supercontinuum laser (NKT photonics) and DAPI was excited using a 405 nm diode laser controlled by a PDL800-B module (PicoQuant). Channels were imaged sequentially with a pixel size between 90 and 110 nm. Presented images are projections of 6-10 z-planes, processed in ImageJ.

Acknowledgements: We thank S. Doxsey, M. Mishima, J. Peränen and J. Pasterkamp for the gift of materials, and Dr. J. Demmers (Erasmus MC, Rotterdam) for the help with mass spectrometry experiments. This work was supported by the Netherlands Organization for Scientific Research grant CW ECHO 711.011.005 to A. A and A. J. R. H., and by the Proteins@Work, a program of the Netherlands Proteomics Centre financed by the Netherlands Organization for Scientific Research (NWO) as part of the National Roadmap Large-scale Research Facilities of the Netherlands (project number 184.032.201).

Conflict of interest: The authors declare that they have no conflicts of interest with the contents of this article.

Author Contributions

AA conceived and coordinated the study and wrote the paper. QL, FL, KLY and AS-M designed, performed and analyzed the experiments. LCK and AJRH contributed to the coordination of the study, data analysis and writing the paper. RT, IG and SR provided technical assistance with the experiments and their analysis and contributed to the preparation of the figures. All authors reviewed the results and approved the final version of the manuscript.

REFERENCES

1. Mierzwa, B., and Gerlich, D. W. (2014) Cytokinetic abscission: molecular mechanisms and temporal control. *Dev Cell* **31**, 525-538
2. Green, R. A., Paluch, E., and Oegema, K. (2012) Cytokinesis in animal cells. *Annu Rev Cell Dev Biol* **28**, 29-58
3. Glotzer, M. (2009) The 3Ms of central spindle assembly: microtubules, motors and MAPs. *Nat Rev Mol Cell Biol* **10**, 9-20
4. White, E. A., and Glotzer, M. (2012) Centralspindlin: at the heart of cytokinesis. *Cytoskeleton (Hoboken)* **69**, 882-892
5. Schiel, J. A., and Prekeris, R. (2013) Membrane dynamics during cytokinesis. *Curr Opin Cell Biol* **25**, 92-98
6. Gould, G. W. (2015) Animal cell cytokinesis: The role of dynamic changes in the plasma membrane proteome and lipidome. *Semin Cell Dev Biol* **53**, 64-73
7. Albertson, R., Riggs, B., and Sullivan, W. (2005) Membrane traffic: a driving force in cytokinesis. *Trends Cell Biol* **15**, 92-101
8. Grigoriev, I., Yu, K. L., Martinez-Sanchez, E., Serra-Marques, A., Smal, I., Meijering, E., Demmers, J., Peranen, J., Pasterkamp, R. J., van der Sluijs, P., Hoogenraad, C. C., and Akhmanova, A. (2011) Rab6, Rab8, and MICAL3 Cooperate in Controlling Docking and Fusion of Exocytotic Carriers. *Curr Biol* **21**, 967-974
9. Ang, A. L., Folsch, H., Koivisto, U. M., Pypaert, M., and Mellman, I. (2003) The Rab8 GTPase selectively regulates AP-1B-dependent basolateral transport in polarized Madin-Darby canine kidney cells. *J Cell Biol* **163**, 339-350
10. Henry, L., and Sheff, D. R. (2008) Rab8 regulates basolateral secretory, but not recycling, traffic at the recycling endosome. *Mol Biol Cell* **19**, 2059-2068
11. Knodler, A., Feng, S., Zhang, J., Zhang, X., Das, A., Peranen, J., and Guo, W. (2010) Coordination of Rab8 and Rab11 in primary ciliogenesis. *Proc Natl Acad Sci U S A* **107**, 6346-6351
12. Kaplan, A., and Reiner, O. (2011) Linking cytoplasmic dynein and transport of Rab8 vesicles to the midbody during cytokinesis by the doublecortin domain-containing 5 protein. *J Cell Sci* **124**, 3989-4000
13. Schiel, J. A., Simon, G. C., Zaharris, C., Weisz, J., Castle, D., Wu, C. C., and Prekeris, R. (2012) FIP3-endosome-dependent formation of the secondary ingression mediates ESCRT-III recruitment during cytokinesis. *Nat Cell Biol* **14**, 1068-1078
14. Guizetti, J., Schermelleh, L., Mantler, J., Maar, S., Poser, I., Leonhardt, H., Muller-Reichert, T., and Gerlich, D. W. (2011) Cortical constriction during abscission involves helices of ESCRT-III-dependent filaments. *Science* **331**, 1616-1620
15. Hida, Y., and Ohtsuka, T. (2010) CAST and ELKS proteins: structural and functional determinants of the presynaptic active zone. *J Biochem* **148**, 131-137
16. Kolk, S. M., and Pasterkamp, R. J. (2007) MICAL flavoprotein monooxygenases: structure, function and role in semaphorin signaling. *Adv Exp Med Biol* **600**, 38-51
17. Terman, J. R., Mao, T., Pasterkamp, R. J., Yu, H. H., and Kolodkin, A. L. (2002) MICALs, a family of conserved flavoprotein oxidoreductases, function in plexin-mediated axonal repulsion. *Cell* **109**, 887-900
18. Giridharan, S. S., and Caplan, S. (2014) MICAL-family proteins: Complex regulators of the actin cytoskeleton. *Antioxid Redox Signal* **20**, 2059-2073
19. Fukuda, M., Kanno, E., Ishibashi, K., and Itoh, T. (2008) Large scale screening for novel rab effectors reveals unexpected broad Rab binding specificity. *Mol Cell Proteomics* **7**, 1031-1042
20. de Boer, E., Rodriguez, P., Bonte, E., Krijgsveld, J., Katsantoni, E., Heck, A., Grosveld, F., and Strouboulis, J. (2003) Efficient biotinylation and single-step purification of tagged transcription factors in mammalian cells and transgenic mice. *Proc Natl Acad Sci U S A* **100**, 7480-7485.

21. Bennett, V., and Baines, A. J. (2001) Spectrin and ankyrin-based pathways: metazoan inventions for integrating cells into tissues. *Physiol Rev* **81**, 1353-1392
22. Baines, A. J. (2009) Evolution of spectrin function in cytoskeletal and membrane networks. *Biochem Soc Trans* **37**, 796-803
23. Bennett, V., and Healy, J. (2009) Membrane domains based on ankyrin and spectrin associated with cell-cell interactions. *Cold Spring Harb Perspect Biol* **1**, a003012
24. Maliga, Z., Junqueira, M., Toyoda, Y., Ettinger, A., Mora-Bermudez, F., Klemm, R. W., Vasilj, A., Guhr, E., Ibarlucea-Benitez, I., Poser, I., Bonifacio, E., Huttner, W. B., Shevchenko, A., and Hyman, A. A. (2013) A genomic toolkit to investigate kinesin and myosin motor function in cells. *Nat Cell Biol* **15**, 325-334
25. Liu, F., Rijkers, D. T., Post, H., and Heck, A. J. (2015) Proteome-wide profiling of protein assemblies by cross-linking mass spectrometry. *Nat Methods* **12**, 1179-1184
26. Schmidt, E. F., Shim, S. O., and Strittmatter, S. M. (2008) Release of MICAL autoinhibition by semaphorin-plexin signaling promotes interaction with collapsin response mediator protein. *J Neurosci* **28**, 2287-2297
27. Ran, F. A., Hsu, P. D., Wright, J., Agarwala, V., Scott, D. A., and Zhang, F. (2013) Genome engineering using the CRISPR-Cas9 system. *Nat Protoc* **8**, 2281-2308
28. Bassi, Z. I., Audusseau, M., Riparbelli, M. G., Callaini, G., and D'Avino, P. P. (2013) Citron kinase controls a molecular network required for midbody formation in cytokinesis. *Proc Natl Acad Sci U S A* **110**, 9782-9787
29. Mishima, M., Kaitna, S., and Glotzer, M. (2002) Central spindle assembly and cytokinesis require a kinesin-like protein/RhoGAP complex with microtubule bundling activity. *Dev Cell* **2**, 41-54
30. Makyio, H., Ohgi, M., Takei, T., Takahashi, S., Takatsu, H., Katoh, Y., Hanai, A., Ueda, T., Kanaho, Y., Xie, Y., Shin, H. W., Kamikubo, H., Kataoka, M., Kawasaki, M., Kato, R., Wakatsuki, S., and Nakayama, K. (2012) Structural basis for Arf6-MKLP1 complex formation on the Flemming body responsible for cytokinesis. *EMBO J* **31**, 2590-2603
31. Joseph, N., Hutterer, A., Poser, I., and Mishima, M. (2012) ARF6 GTPase protects the post-mitotic midbody from 14-3-3-mediated disintegration. *EMBO J* **31**, 2604-2614
32. Zhao, W. M., Seki, A., and Fang, G. (2006) Cep55, a microtubule-bundling protein, associates with centralspindlin to control the midbody integrity and cell abscission during cytokinesis. *Mol Biol Cell* **17**, 3881-3896
33. Reinecke, J. B., Katafiasz, D., Naslavsky, N., and Caplan, S. (2015) Novel Functions for the Endocytic Regulatory Proteins MICAL-L1 and EHD1 in Mitosis. *Traffic* **16**, 48-67
34. Kouranti, I., Sachse, M., Arouche, N., Goud, B., and Echard, A. (2006) Rab35 regulates an endocytic recycling pathway essential for the terminal steps of cytokinesis. *Curr Biol* **16**, 1719-1725
35. Dambournet, D., Machicoane, M., Chesneau, L., Sachse, M., Rocancourt, M., El Marjou, A., Formstecher, E., Salomon, R., Goud, B., and Echard, A. (2011) Rab35 GTPase and OCRL phosphatase remodel lipids and F-actin for successful cytokinesis. *Nat Cell Biol* **13**, 981-988
36. Goss, J. W., and Toomre, D. K. (2008) Both daughter cells traffic and exocytose membrane at the cleavage furrow during mammalian cytokinesis. *J Cell Biol* **181**, 1047-1054
37. Gromley, A., Yeaman, C., Rosa, J., Redick, S., Chen, C. T., Mirabelle, S., Guha, M., Sillibourne, J., and Doxsey, S. J. (2005) Centriolin anchoring of exocyst and SNARE complexes at the midbody is required for secretory-vesicle-mediated abscission. *Cell* **123**, 75-87
38. Grigoriev, I., Splinter, D., Keijzer, N., Wulf, P. S., Demmers, J., Ohtsuka, T., Modesti, M., Maly, I. V., Grosveld, F., Hoogenraad, C. C., and Akhmanova, A. (2007) Rab6 regulates transport and targeting of exocytotic carriers. *Dev Cell* **13**, 305-314
39. Neef, R., Klein, U. R., Kopajtich, R., and Barr, F. A. (2006) Cooperation between mitotic kinesins controls the late stages of cytokinesis. *Curr Biol* **16**, 301-307

40. Peranen, J., Auvinen, P., Virta, H., Wepf, R., and Simons, K. (1996) Rab8 promotes polarized membrane transport through reorganization of actin and microtubules in fibroblasts. *J Cell Biol* **135**, 153-167
41. Kao, A., Chiu, C. L., Vellucci, D., Yang, Y., Patel, V. R., Guan, S., Randall, A., Baldi, P., Rychnovsky, S. D., and Huang, L. (2011) Development of a novel cross-linking strategy for fast and accurate identification of cross-linked peptides of protein complexes. *Mol Cell Proteomics* **10**, M110 002212

FOOTNOTES

The abbreviations used are**:** MKLP1, Mitotic Kinesin-Like Protein 1; bioGFP, a GFP tag with an N-terminally attached peptide that can be biotinylated; DSSO**,** disuccinimidyl sulfoxide; CRIK, Citron kinase; PEI, polyethylenimine; gRNAs**,** guide RNAs; PBS, phosphate-buffered saline; MO, monooxygenase domain; CH, calponin homology domain; LIM, Lin11, Isl-1, and Mec-3 domain (zinc binding); CC, predicted coiled coil; MD, kinesin motor domain.

FIGURE LEGENDS

Figure 1. Cross-linking mass spectrometry analysis of MICAL3 -MKLP1 comlpex.
A. Mass spectrometry-based analysis of streptavidin pull down assay with the extracts of HEK293T cells expressing bioGFP-MICAL3 and BirA.
B. Schematic map of intraprotein cross-links in MICAL3 (red lines). Abbreviations for protein domains: MO, monooxygenase domain; CH, calponin homology domain; LIM, Lin11, Isl-1, and Mec-3 domain (zinc binding); CC, predicted coiled coil. The cross-links identified within MO domain, which are labeled with red dashed lines, were mapped onto mouse MICAL1 monooxygenase structure (PDB, 4TXI). The cross-links are within the DSSO maximal distance constraint of 28.4 Å.
C. Schematic map of intraprotein cross-links MKLP1 (red lines). Abbreviations for protein domains: MD, kinesin motor domain; CC, predicted coiled coil; D7, amino acids deleted in the D7 mutant; D8, amino acids deleted in the D8 mutant; ARF6, ARF6-binding region. The cross-link identified within ARF6 binding domain, which is labeled with red dashed line, was mapped onto the mouse ARF6-MKLP1 complex structure (PDB, 3VHX). The cross-link is within the DSSO maximal distance constraint of 28.4 Å. The amino acids sequence 531-960 of MKLP1 is shown. CC is highlighted in purple (535-620). ARF6 binding region is highlighted in blue (794-911). Lysines cross-linked lysines with MICAL3 are highlighted in yellow. The underlined lysines indicate intraprotein cross-links. D7 and D8 deletions are underlined in black and grey, respectively. Aurora B phosphorylation site (S812) is indicated by a black box.

Figure 2. Mapping of the domains in MICAL3 required for the interaction with MKLP1.
A. Schematic map of MICAL3-MKLP1 complex based on interprotein cross-links (red lines).
B. Schematic overview of MICAL3 deletion mutants used in this study and a summary of identified interactions. Numbering is based on MICAL3 isoform 1 (NP_056056). Binding regions for the known partners of MICAL3 are indicated.
C-E, Streptavidin pull-down assays performed with the extracts of HEK293T cells co-expressing BirA, BioGFP, or the indicated MICAL3 or MKLP1 constructs. Antibodies against GFP, mCherry or MKLP1 were used for Western blotting, as indicated.

Figure 3. Mapping of the domains in MKLP1 required for the interaction with MICAL3.
A. Schematic overview of MKLP1 deletion mutants used in this study and a summary of identified interactions. Numbering is based on MKLP1 isoform 1 (NCBI protein NP_612565). Binding regions for the known partners of MKLP1 are indicated.
B-D, Streptavidin pull-down assays performed with the extracts of HEK293T cells co-expressing BirA, BioGFP, or the indicated MICAL3 or MKLP1 constructs. Antibodies against GFP or mCherry were used for Western blotting, as indicated. An empty lane cropped in D is indicated by a dashed line.

Figure 4. MKLP1 recruits MICAL3 to the central spindle and the midbody.
A-C. Localization of endogenous MICAL3 (A, green), mCherry-MICAL3-WT (B, red) or mCherry-MICAL3-3G3W (C, red) during cytokinesis. HeLa cells were stained with the indicated antibodies. Cell outlines are indicated by dashed lines. Insets, magnifications of the boxed areas.
D,E. Western blots (D) and quantification of normalized immunoblot values (E) for MKLP1 expression in HeLa cells 72 hrs after transfection with the control (luciferase) or MKLP1 siRNAs. **, $p<0.01$, Student's *t*-test based on 3 independent experiments.
F,I. Immunostaining of MICAL3 (F) or MKLP1 (I) (green) and α-tubulin (red) in HeLa cells 72 hrs after transfection with the indicated siRNAs. Insets, magnifications of the boxed areas.
G. Relative intensity of MICAL3 at the central spindle compared to cytoplasm in control and MKLP1 knockdown cells. The red dashed line indicates the background level, equal to 1. ***, $p<0.001$, Mann-Whitney U test. More than 20 cells analysed from 3 independent experiments.

H. Western blots of extracts of control and MICAL3 knockout HeLa cells. Additional samples present on the gel were cropped as indicated by a dashed line.

Figure 5. Cytokinesis defects in MICAL3 knockout cells.

A. Phase-contrast-based live imaging of control and MICAL3 knockout cells. Insets show magnifications of intercellular bridges or cell membrane (arrows). See also Movies S1-S3.

B-D. Time interval between mitosis onset and furrow initiation (B), abscission time (C) and percentage of the cells which fused back without completing cytokinesis (D) in control and MICAL3 knockout cells. Data represent more than 150 cells from 3 independent experiments, **, $p<0.01$, ***, $p<0.001$, Student's *t*-test.

E. Immunostaining of α-tubulin (green) and DAPI (blue) in control or MICAL3 knockout cells, with binucleated cells indicated with white arrows, and quantification of the percentage of bi- and multinucleated cells in control and MICAL3 knockout cells. Data represent more than 1000 cells from 3 independent experiments, ***, $p<0.001$, Student's *t*-test.

F,G. Percentage of binucleated cells determined by counting GFP-positive cells in rescue experiments of MICAL3 knockout (F) or MKLP1 knockdown (G) with the indicated constructs. Data represent more than 3000 cells from 4 or 5 independent experiments, *, $p<0.05$, **, $p<0.01$, ***, $p<0.001$, n.s., $p>0.05$, Student's *t*-test.

H. Immunostaining of BioGFP-MKLP1-D7/D8 (green) and MICAL3 (red) in MKLP1 knockdown cells. Cell outlines are indicated by dashed lines. Magnified midbody images are shown in insets.

Figure 6. Actin distribution in MICAL3 knockout cells.

A. Immunostaining of MICAL3 (green) and actin (red) in control or MICAL3 knockout cells. Insets, magnifications of the boxed areas.

B. Ratio of the intensity of actin at midzone to intensity in the cytoplasm in control or MICAL3 knockout cells at different stages of cytokinesis. Around 100 cells were analysed in 3 independent experiments. n.s., $P>0.05$, Mann-Whitney U test.

Figure 7. MICAL3 is required for ELKS localization to the midbody.

A, Immunostaining of ELKS (green) and α-tubulin (red) in control or MICAL3 knockout cells. Insets, magnified midbody images.

B. Percentage of cells with detectable specific ELKS staining at the midbody in control and MICAL3 knockout cells. Data represent 60 cells from 3 independent experiments. **, $p<0.01$, Student's *t*-test.

C. Mass spectrometry-based analysis of streptavidin pull down assay with the extracts of HEK293T cells expressing biotinylation-tagged ELKS and BirA.

D. Streptavidin pull-down assays performed with the extracts of HEK293T cells co-expressing BirA and the indicated proteins, analyzed by Western blotting with antibodies against GFP or mCherry.

Figure 8. MICAL3, Rab8A and ELKS act in the same cytokinesis pathway.

A,D-F. Immunostaining of Rab8A (A), transferrin receptor (TfR) (D), GFP-Rab11 (E) or CRIK (F) (green) and α-tubulin (A, E), actin (D) or KIF14 (F) (red) in control or the indicated knockout or knockdown cells. Cell outlines are indicated by dashed lines. Insets, magnified midbody images.

B. Percentage of cells with detectable specific Rab8A staining at the midbody in control and MICAL3 knockout cells. Data represent 60 cells from 3 independent experiments. *, $p<0.05$, Student's *t*-test.

C,I. Relative intensity of Rab8A at the midbody compared to cytoplasm in the indicated control, knockout or knockdown cells. The red dashed line indicates background level, equal to 1. 15 to 40 cells were analysed in 3 independent experiments. ***, $p<0.001$, Mann-Whitney U test.

G,H. Western blots of extracts of HeLa cells after 72 hrs of transfection with the indicated siRNAs.
J,K. Percentage of bi- and multinucleated cells after transfection with the indicated siRNAs. Data represent more than 2000 cells from 3 independent experiments; **, $p<0.01$, ***, $p<0.001$, Student's *t*-test.

Figure 9. A model for MICAL3 function during cytokinesis.
Schematic representation of the model described in this study. MKLP1 localizes to the midbody and recruits MICAL3, which in turn participates in recruiting ELKS and Rab8A-bound vesicles. As a complex, they promote maturation of the intercellular bridge and abscission.

A

Rank	Protein name	Accession number	Unique peptides
1	MICAL3	Q7RTP6	149
2	SPTBN1	Q01082	58
3	SPTAN	Q13813	54
4	KIF23	Q02241	48
5	RACGAP	Q9H0H5	36
6	NINL	Q9Y2I6	25
7	CSNK2A2	P19784	19
8	TUBA1B	P68363	1
9	SHCBP1	Q8NEM2	17
10	ERC1	Q8IUD2	15
11	PGAM5	Q96HS1	15
12	CSNK2B	P67870	10
13	RAB8A	P61006	9
14	SLC25A	P12235	1
15	CD2AP	Q9Y5K6	9
16	CCHCR1	Q8TD31	9
17	ANAPC1	Q9H1A4	9
18	ANK3	Q12955	9
19	HAX1	O00165	8
20	TAF6L	Q9Y6J9	8

C

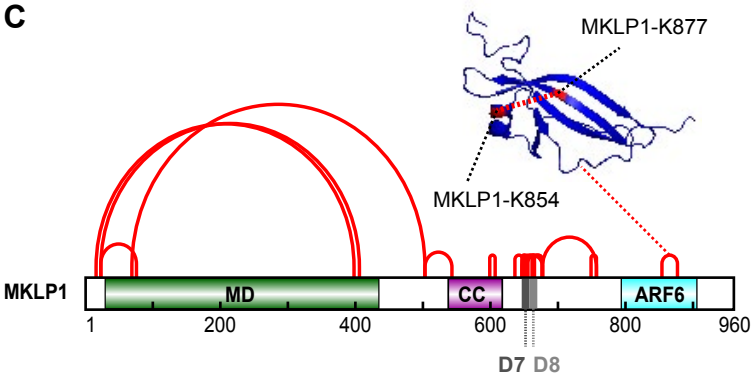


```
531  NAVLSKENHM QGKLNEKEKM ISGQKLEIER LEKKNKTLEY KIEILEKTTT IYEEDKRNLQ

591  QELETQNQKL QRQFSDKRRL EARLQGMVTE TTMKWEKECE RRVAAKQLEM QNKLWVKDEK

651  LKQLKAIVTE PKTEKPERPS RERDREKVTQ RSVSPSPVPL SSNYIAQISN GQQLMSQPQL
                D7                D8

711  HRRSNSCSSI SVASCISEWE QKIPTYNTPL KVTSIARRRQ QEPGQSKTCI VSDRRRGMYW

771  TEGREVVPTF RNEIEIEEDH CGRLLFQPDQ NAPPIRLRHR RSRSAGDRWV DHKPASNMQT

831  ETVMQPHVPH AITVSVANEK ALAKCEKYML THQELASDGE IETKLIKGDI YKTRGGGQSV

891  QFTDIETLKQ ESPNGSRKRR SSTVAPAQPD GAESEWTDVE TRCSVAVEMR AGSQLGPGYQ

951  HHAQPKRKKP
```

B

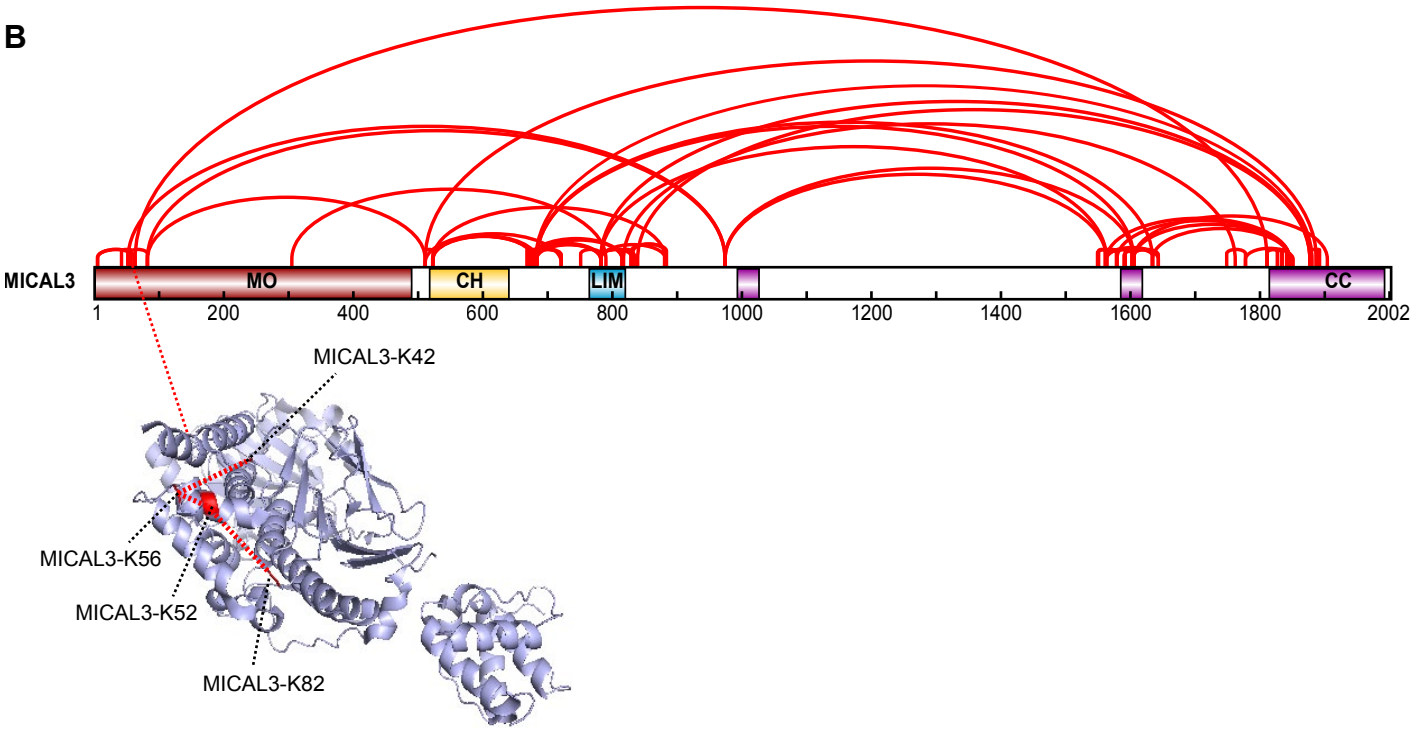

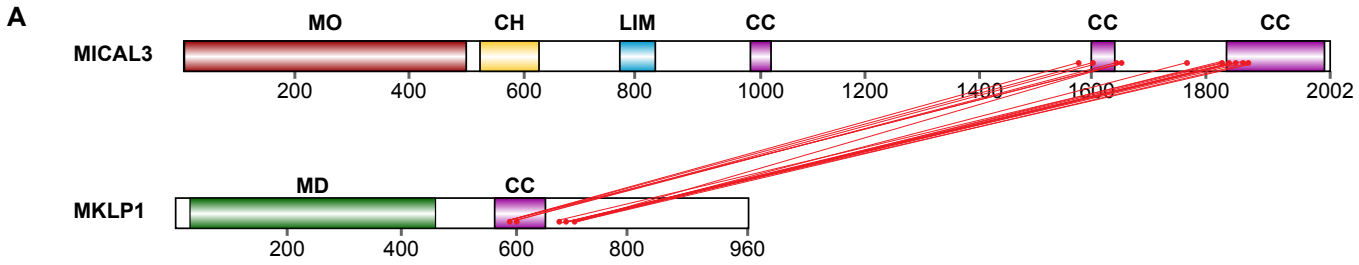

B

Protein	Amino Acids	Interaction
MICAL3	1-1918	MKLP1
MICAL3-WT	1-1918	+
MICAL3-3G3W	1-1918	+
MICAL3-CC1	1019-1918	+
MICAL3-CC2	1090-1735	–
MICAL3-CC3	1457-1918	+
MICAL3-CC4	1735-1918	+
MICAL3-WT-N1	1-1712	–

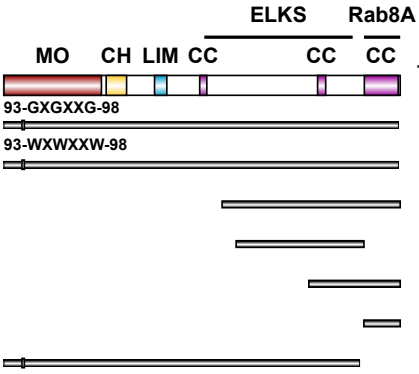

C

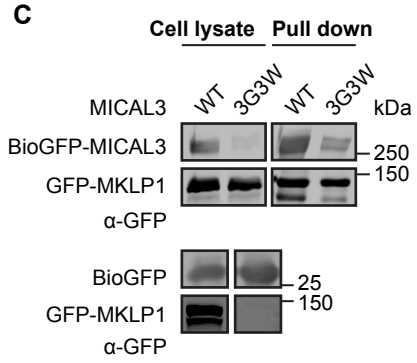

D

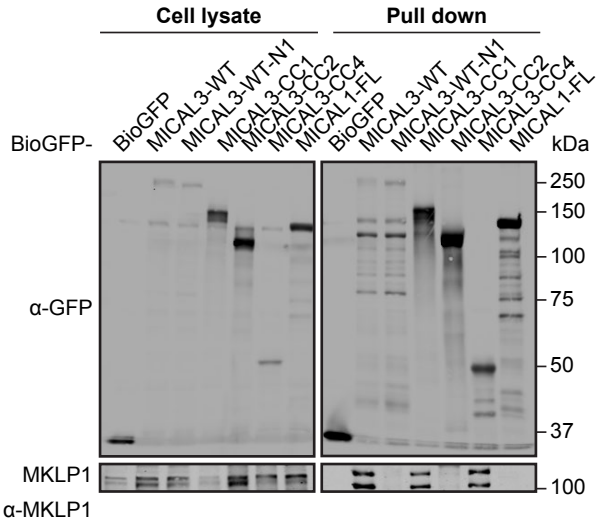

E

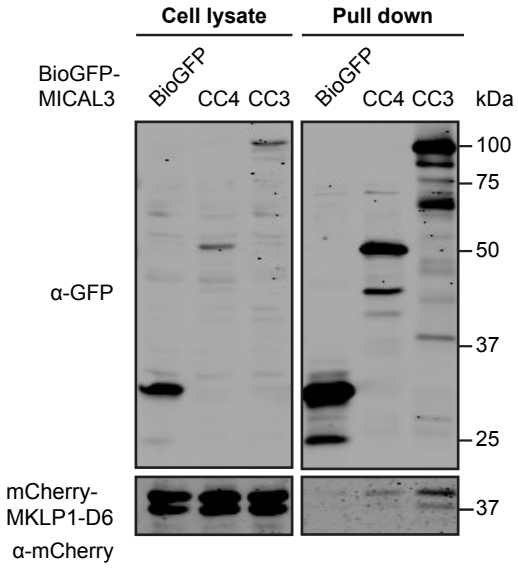

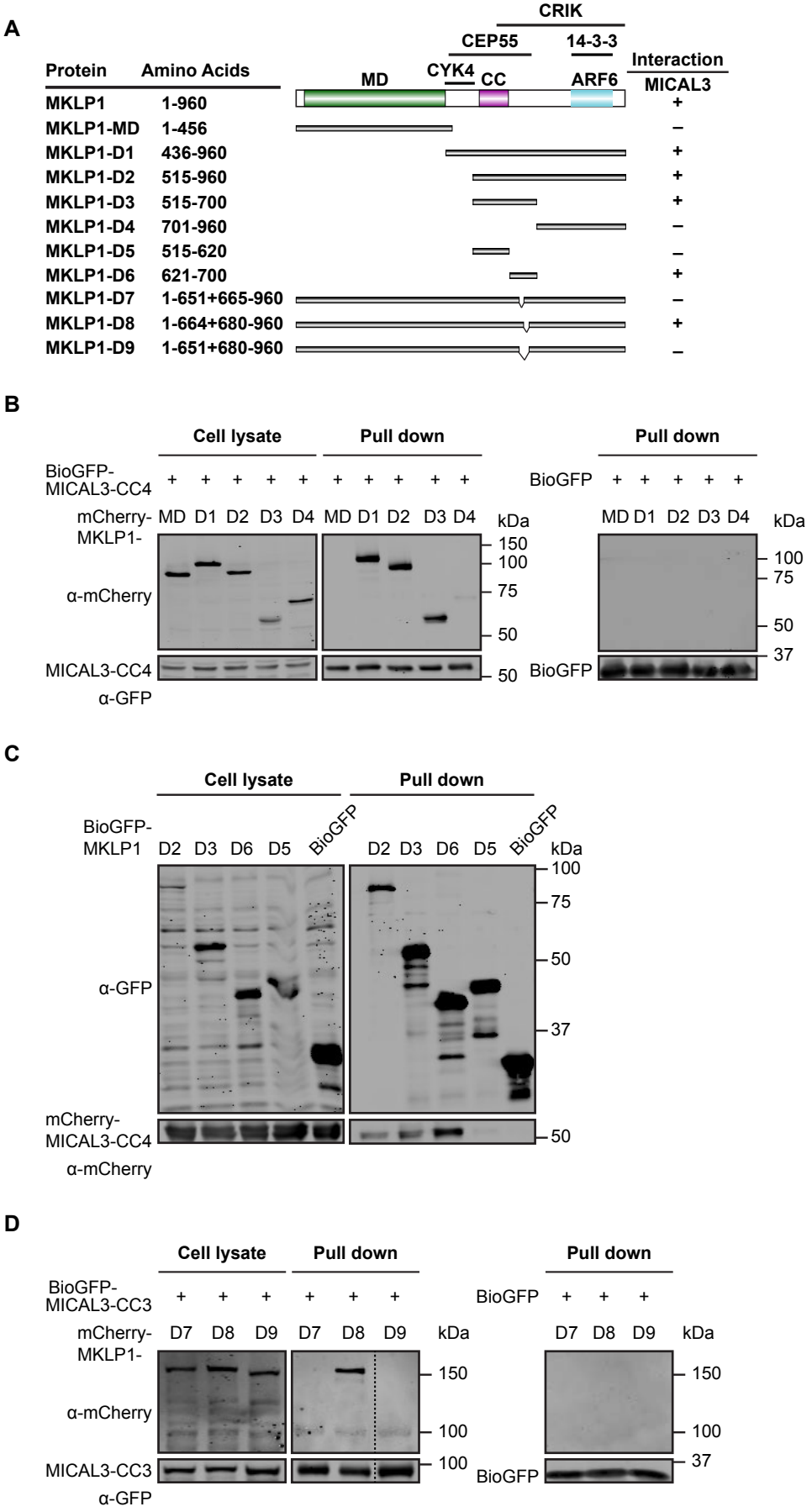
A
CRIK
CEP55
14-3-3
Protein
Amino Acids
MD
CYK4
CC
ARF6
Interaction
MICAL3
MKLP1 1-960 +
MKLP1-MD 1-456 –
MKLP1-D1 436-960 +
MKLP1-D2 515-960 +
MKLP1-D3 515-700 +
MKLP1-D4 701-960 –
MKLP1-D5 515-620 –
MKLP1-D6 621-700 +
MKLP1-D7 1-651+665-960 –
MKLP1-D8 1-664+680-960 +
MKLP1-D9 1-651+680-960 –
B
Cell lysate
Pull down
Pull down
BioGFP-MICAL3-CC4
BioGFP
mCherry-MKLP1-
MD D1 D2 D3 D4 MD D1 D2 D3 D4 kDa
MD D1 D2 D3 D4 kDa
150
100
75
50
100
75
50
37
α-mCherry
MICAL3-CC4
BioGFP
50
α-GFP
C
Cell lysate
Pull down
BioGFP-MKLP1
D2 D3 D6 D5 BioGFP
D2 D3 D6 D5 BioGFP kDa
100
75
50
37
α-GFP
mCherry-MICAL3-CC4
50
α-mCherry
D
Cell lysate
Pull down
Pull down
BioGFP-MICAL3-CC3
BioGFP
mCherry-MKLP1-
D7 D8 D9 D7 D8 D9 kDa
D7 D8 D9 kDa
150
100
150
100
37
α-mCherry
MICAL3-CC3
100
BioGFP
α-GFP

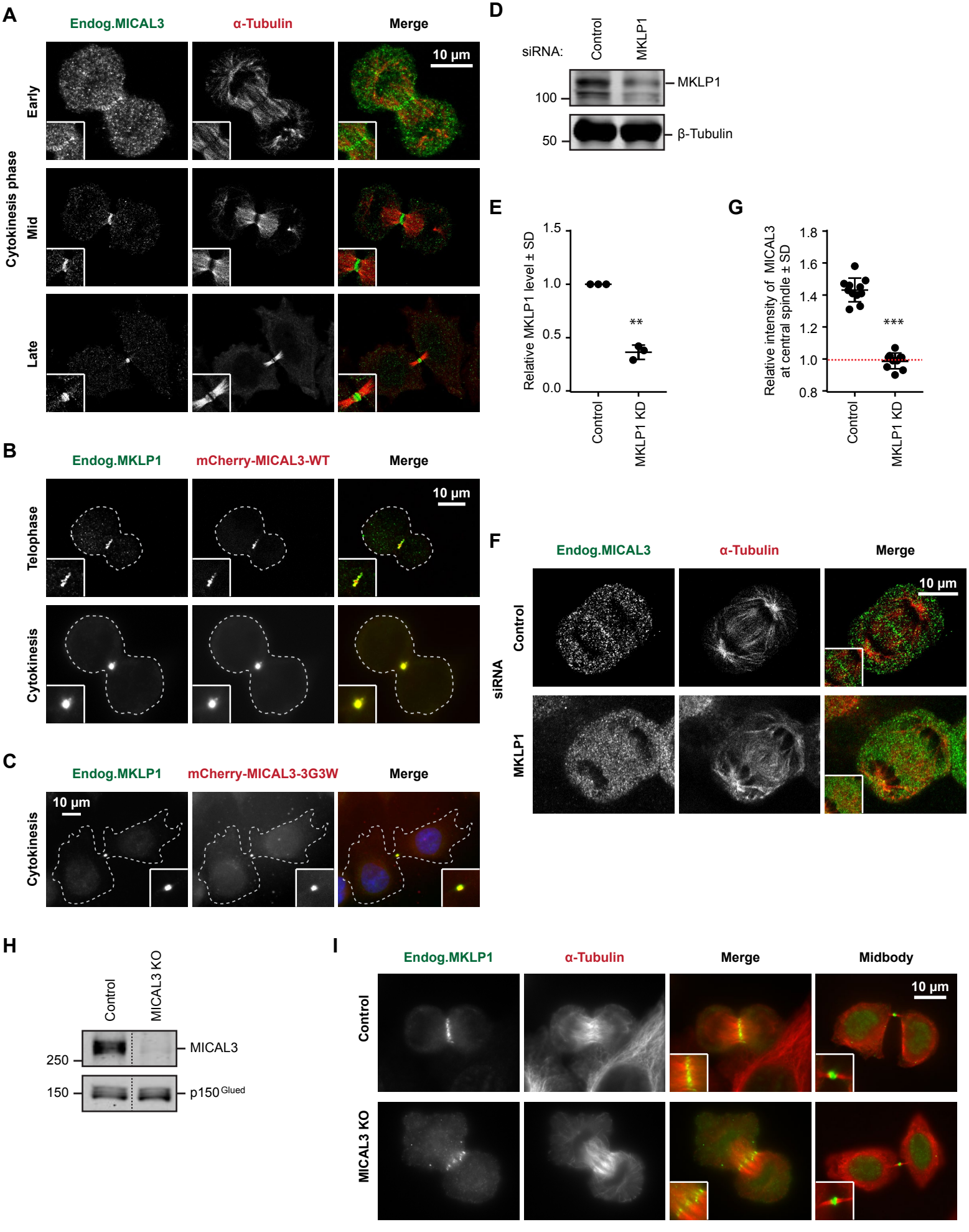
A
Endog.MICAL3
α-Tubulin
Merge
Cytokinesis phase
Early
Mid
Late
10 μm
B
Endog.MKLP1
mCherry-MICAL3-WT
Merge
Telophase
Cytokinesis
10 μm
C
Endog.MKLP1
mCherry-MICAL3-3G3W
Merge
Cytokinesis
10 μm
D
siRNA:
Control
MKLP1
100
50
MKLP1
β-Tubulin
E
Relative MKLP1 level ± SD
1.5
1.0
0.5
0.0
**
Control
MKLP1 KD
G
Relative intensity of MICAL3 at central spindle ± SD
1.8
1.6
1.4
1.2
1.0
0.8
***
Control
MKLP1 KD
F
Endog.MICAL3
α-Tubulin
Merge
siRNA
Control
MKLP1
10 μm
H
Control
MICAL3 KO
250
150
MICAL3
p150 Glued
I
Endog.MKLP1
α-Tubulin
Merge
Midbody
Control
MICAL3 KO
10 μm

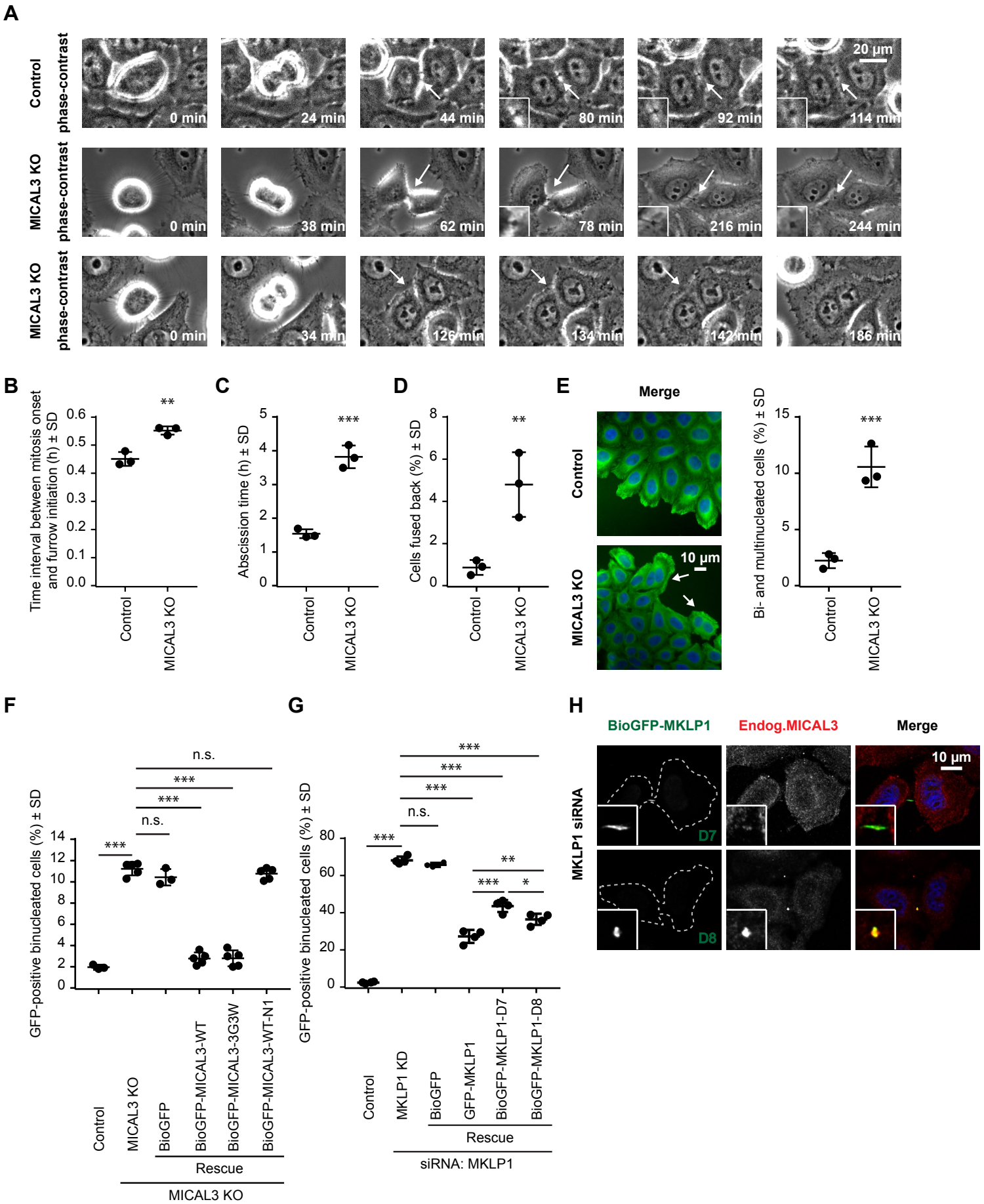
A
Control phase-contrast
MICAL3 KO phase-contrast
MICAL3 KO phase-contrast
0 min
24 min
44 min
80 min
92 min
20 µm
114 min
0 min
38 min
62 min
78 min
216 min
244 min
0 min
34 min
126 min
134 min
142 min
186 min
B
Time interval between mitosis onset and furrow initiation (h) ± SD
Control
MICAL3 KO
C
Abscission time (h) ± SD
D
Cells fused back (%) ± SD
E
Merge
Control
MICAL3 KO
10 µm
Bi- and multinucleated cells (%) ± SD
F
GFP-positive binucleated cells (%) ± SD
Control
MICAL3 KO
BioGFP
BioGFP-MICAL3-WT
BioGFP-MICAL3-3G3W
BioGFP-MICAL3-WT-N1
Rescue
MICAL3 KO
n.s.
G
GFP-positive binucleated cells (%) ± SD
Control
MKLP1 KD
BioGFP
GFP-MKLP1
BioGFP-MKLP1-D7
BioGFP-MKLP1-D8
Rescue
siRNA: MKLP1
H
BioGFP-MKLP1
Endog.MICAL3
Merge
MKLP1 siRNA
D7
D8
10 µm

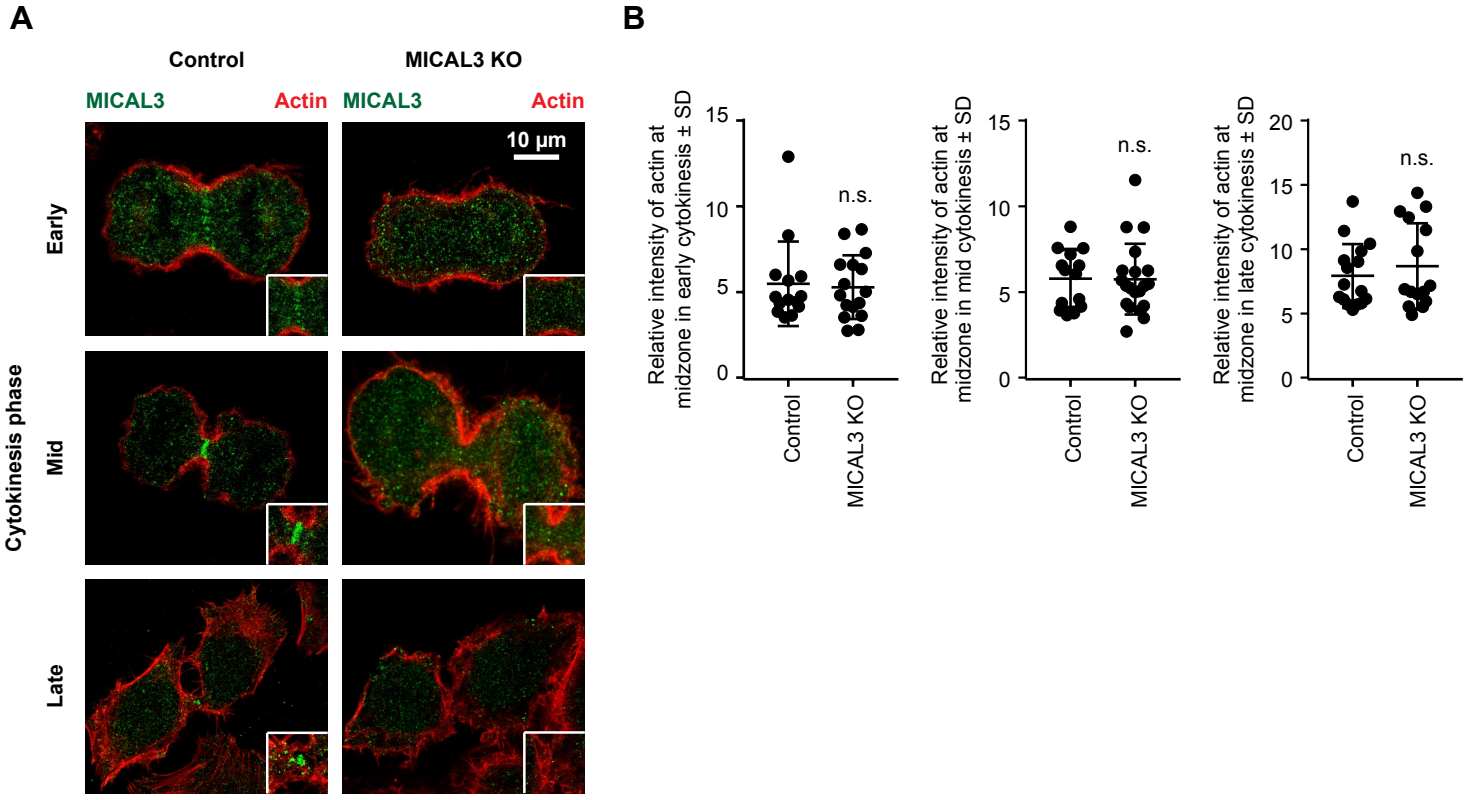
A
Control
MICAL3 KO
MICAL3
Actin
MICAL3
Actin
10 μm
Cytokinesis phase
Early
Mid
Late
B
Relative intensity of actin at midzone in early cytokinesis ± SD
15
10
5
0
n.s.
Control
MICAL3 KO
Relative intensity of actin at midzone in mid cytokinesis ± SD
15
10
5
0
n.s.
Control
MICAL3 KO
Relative intensity of actin at midzone in late cytokinesis ± SD
20
15
10
5
0
n.s.
Control
MICAL3 KO

A

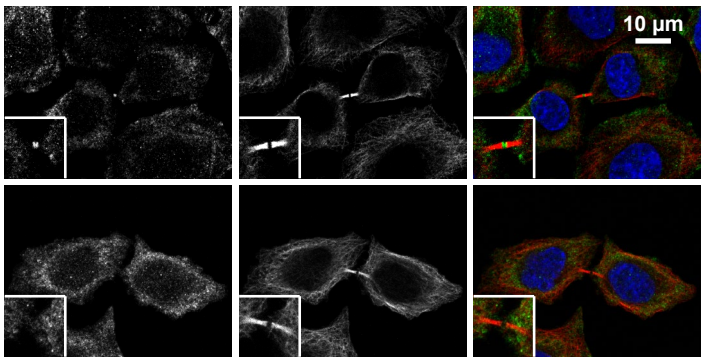

B

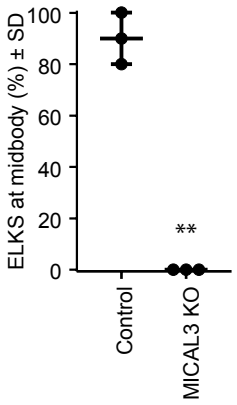

C

Rank	Protein name	Accession number	Unique peptides
1	ERC1	Q8IUD2	2643
2	ERC2	O15083	550
4	MICAL3	Q7RTP6	80
32	CRIK	O14578	33
89	KIF23	Q02241	12
123	KIF14	Q15058	9

D

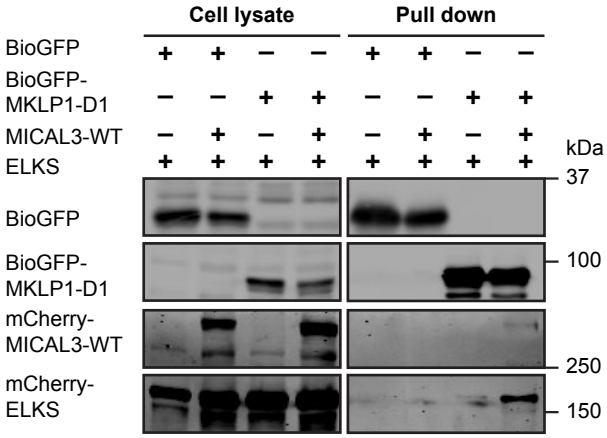

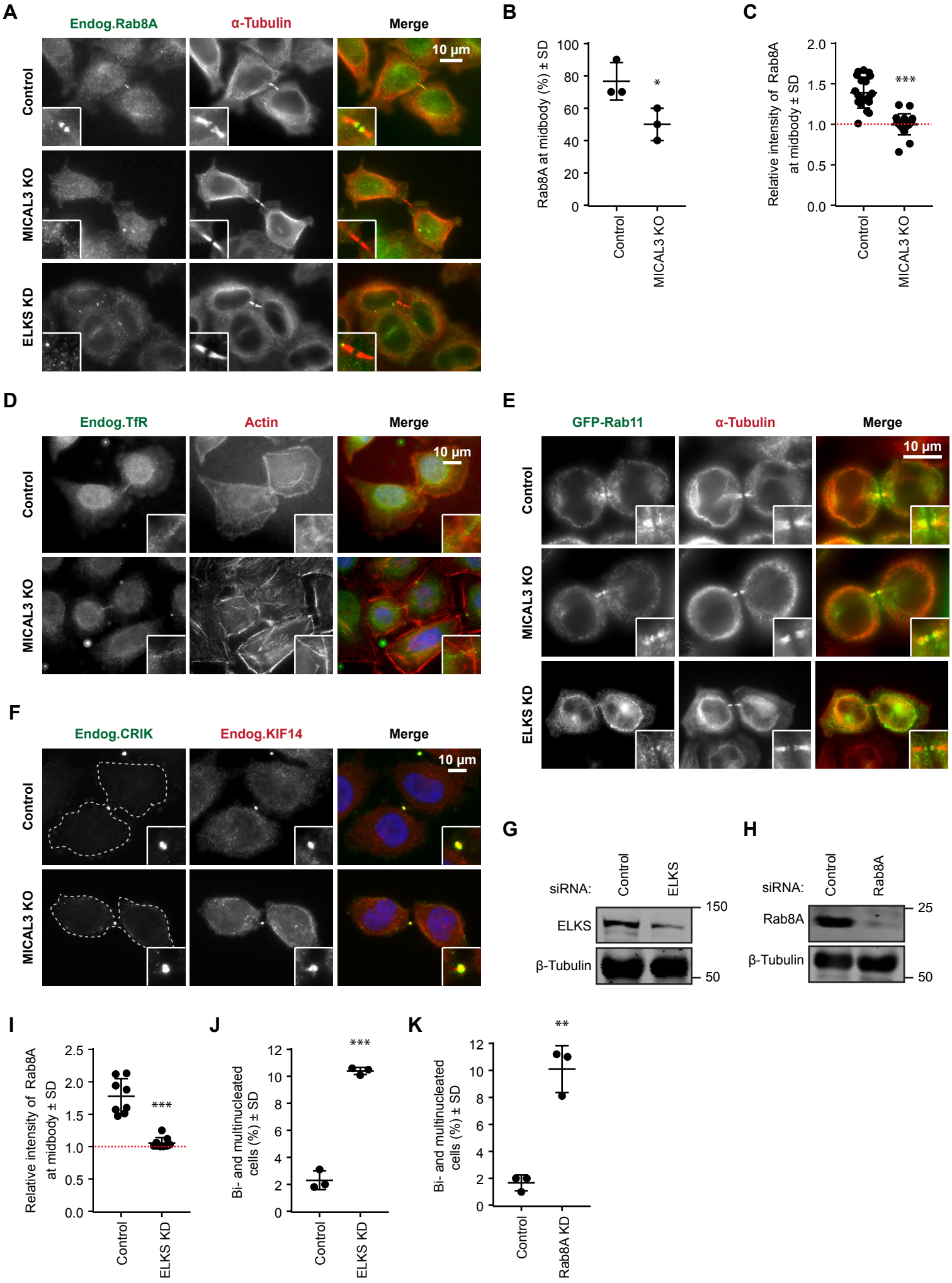
A
Endog.Rab8A
α-Tubulin
Merge
10 μm
Control
MICAL3 KO
ELKS KD
B
Rab8A at midbody (%) ± SD
100
80
60
40
20
0
*
Control
MICAL3 KO
C
Relative intensity of Rab8A at midbody ± SD
2.0
1.5
1.0
0.5
0.0
***
Control
MICAL3 KO
D
Endog.TfR
Actin
Merge
10 μm
Control
MICAL3 KO
E
GFP-Rab11
α-Tubulin
Merge
10 μm
Control
MICAL3 KO
ELKS KD
F
Endog.CRIK
Endog.KIF14
Merge
10 μm
Control
MICAL3 KO
G
siRNA:
Control
ELKS
ELKS
β-Tubulin
150
50
H
siRNA:
Control
Rab8A
Rab8A
β-Tubulin
25
50
I
Relative intensity of Rab8A at midbody ± SD
2.5
2.0
1.5
1.0
0.5
0.0
***
Control
ELKS KD
J
Bi- and multinucleated cells (%) ± SD
12
10
8
6
4
2
0
***
Control
ELKS KD
K
Bi- and multinucleated cells (%) ± SD
12
10
8
6
4
2
0
**
Control
Rab8A KD

Figure 9 **Liu et al.**

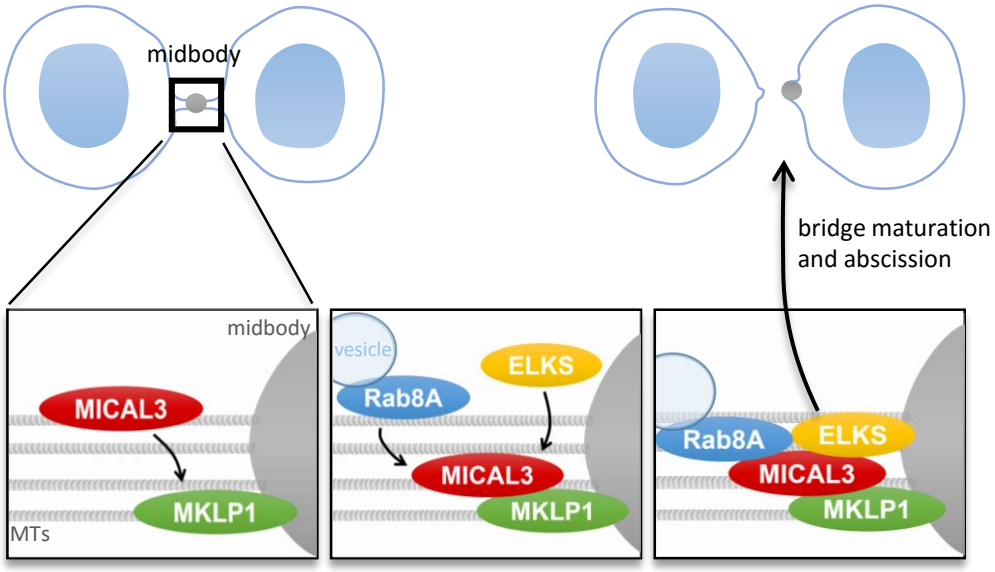

MICAL3 flavoprotein monooxygenase forms a complex with centralspindlin and regulates cytokinesis.

Qingyang Liu, Fan Liu, Ka Lou Yu, Roderick Tas, Ilya Grigoriev, Sanne Remmelzwaal, Andrea Serra-Marques, Lukas C. Kapitein, Albert J.R. Heck and Anna Akhmanova

J. Biol. Chem. published online August 15, 2016
